

# 3D Time-Domain Airborne EM Inversion with Finite-Volume Method

**Xiuyan Ren\***

*Jilin / RMIT University  
Melbourne, Australia  
jdrxy@hotmail.com*

**James Macnae**

*RMIT University  
Melbourne, Australia  
[james.macnae@rmit.edu.au](mailto:james.macnae@rmit.edu.au)*

**Changchun Yin**

*Jilin University  
Changchun, China  
[yinchangchun@jlu.edu.cn](mailto:yinchangchun@jlu.edu.cn)*

**Yunhe Liu**

*Jilin University  
Changchun, China  
[liuyunhe@jlu.edu.cn](mailto:liuyunhe@jlu.edu.cn)*

**Bo Zhang**

*Jilin University  
Changchun, China  
[em\\_zhangbo@163.com](mailto:em_zhangbo@163.com)*

## SUMMARY

We investigate an algorithm for 3D time-domain AEM inversion with the finite-volume and direct Gauss-Newton methods. We separate a spatially varying secondary field from the 1D background in time-domain, and constrain the calculation to be within the small volume of influence of airborne EM secondary source, resulting in more compact discretization. To demonstrate the validity and merits of 3D inversion, we first compare the results with 1D inversion on synthetic data for a horizontal conductor and a dipping plate, which shows that both methods can well recover the horizontal conductor, while only 3D inversion can offer good recovery for the dipping plate. We apply our 3D algorithm to invert GEOTEM data obtained over the Lisheen deposit in Ireland to map the sulphides at depth and obtain similar results to 1D inversion but with better data fitting, further showing the effectiveness of our 3D inversion algorithm.

**Key words:** Time-domain AEM, finite-volume method, 3D, Inversion.

## INTRODUCTION

Airborne electromagnetic (AEM) methods have been used for mineral exploration, geological mapping, underground water and geothermal exploration for years. AEM exploration has quick coverage and dense along-line sampling in any survey area that produce large amounts of data. As a result, imaging and one-dimensional (1D) inversion are always the first choice for data interpretation because they are very fast. Macnae et al. (1991) presented the conductivity-depth imaging for AEM step response and since then 1D inversions such as singular value decomposition (SVD), laterally constrained inversion (LCI), Occam's inversion have been frequently used to interpret AEM data (Chen and Raiche, 1998; Vallée and Smith, 2009; Ley-Cooper et al., 2010; Cai et al., 2014). While these methods are fast and effective when the geology is quasi-layered, in cases in which the earth has severe topography or the earth contains three-dimensional (3D) conductors, 1D inversions cannot deliver reliable 3D geometry of conductors for such geological conditions.

In recent years, many 3D inversion algorithms such as Quasi-Newton, NLCG, Gauss-Newton have been studied for compact 3D exploration targets. Liu and Yin (2016) developed 3D inversion for multipulse airborne transient EM data and they adopted a direct Gauss-Newton method in the inversion with reasonably rapid convergence. Impractical consumptions in time and memory in 3D inversion have greatly limited its use. Concurrently, many acceleration techniques for 3D modelling and inversion have been suggested. Oldenburg et al. (2008) adopted the Multi-frontal Massively Parallel Solver (MUMPS) in the 3D calculation for large-scale multi-source transient EM problems, which saves considerable time in forward modelling and inversions. Yang et al. (2013) investigated a generic parallelization scheme with local meshes that have fine cells near the transmitting source and coarser cells elsewhere. For EM surveys, Druyts et al. (2010) defined the volume of influence (VoI) for AEM transmitters, which is an important concept for 3D model calculation because its volume is much smaller than the entire computing volume under the survey area, and it has sometimes been called footprint (Liu and Becker, 1990; Reid et al., 2006; Yin et al., 2014). The moving footprint concept proposed by Cox and Zhdanov (2007, 2010) has further accelerated the application of 3D inversion. As the 3D secondary field of a compact target has a small range of influence compared to a half-space or layered-earth EM response which we regard as the background field, the spatial extent of the response produced by the geologically anomalous conductor should be much smaller than that of the transmitter VoI. We call this method the time-domain field-separation method and it is used in our 3D calculation.

From a numerical simulation point of view, finite-difference (FD) and finite-element (FE) methods have been well developed. We adopt a finite-volume (FV) method with staggered grids for discretization. With the FV method, we divide the whole region into many discrete sub-volumes without overlap. Compared with FD that uses the difference to replace the derivative, FV is an integral process for each discrete volume element. FE method uses the combination of an interpolation function and node values in each subdivided element to express the variables in the integral, while FV keeps the conservation of variables in each integral with discrete volume elements and has a simple computation process. Jahandari and Farquharson (2014) used an unstructured FV method to solve the frequency-domain EM forward problems, and Oldenburg et al. (2013) developed large-scale time-domain AEM modelling and inversion based on the FV method with staggered grids.

We use the time-domain field-separation method by separating the secondary field (3D conductors) from the background (half-space or layered earth), and adopt the FV method within the small VoI of the secondary source with considerably fewer grids. The background field is easily obtained from 1D algorithms and the actual transmitter current waveform effects can be quantified via convolution. A local mesh and the MUMPS direct solver are used to accelerate the 3D EM calculation. We compare the 3D inversion results with 1D inversions for a synthetic model with a dipping plate and a horizontal rectangular conductor to demonstrate the



Figure 1: (a) staggered grids and control volume; (b) local mesh.

### Inversion theory

We consider the following penalty functional consisting of data misfit and model constraints (Egbert and Kelbert, 2012):

$$\varphi(\tilde{\mathbf{m}}, \mathbf{d}) = (\mathbf{d} - \tilde{\mathbf{f}}(\tilde{\mathbf{m}}))^T (\mathbf{d} - \tilde{\mathbf{f}}(\tilde{\mathbf{m}})) + \gamma \tilde{\mathbf{m}}^T \tilde{\mathbf{m}}, \quad (7)$$

where

$$\tilde{\mathbf{m}} = \mathbf{C}_m^{-1/2} (\mathbf{m} - \mathbf{m}_0) \quad \text{and} \quad \tilde{\mathbf{f}}(\tilde{\mathbf{m}}) = \mathbf{f}(\mathbf{C}_m^{1/2} \tilde{\mathbf{m}} + \mathbf{m}_0), \quad (8)$$

and where in turn  $\mathbf{d}=(d_1, d_2, \dots, d_{N_d})^T$  are the survey data,  $N_d$  is the number of survey data; the model conductivity matrix  $\mathbf{m}=(m_1, m_2, \dots, m_M)^T$  consists of  $M$  parameters;  $\mathbf{m}_0$  is a prior or first guess of model parameters;  $\mathbf{f}(\mathbf{m})$  are non-linear functions in the model space  $\mathbf{m}$ ; the trade-off parameter  $\gamma$  balances the data misfit and model constraints;  $\mathbf{C}_m$  defines the model covariance or regularization term. The data misfit term, it was rescaled from  $(\mathbf{C}_d^{-1/2} \mathbf{d}, \mathbf{C}_d^{-1/2} \mathbf{f})$ , where  $\mathbf{C}_d$  is the covariance of data errors, with its  $i^{\text{th}}$  element being defined as  $0.5 \times (d_i^2 + f_i^2(\mathbf{m}))$  (Wilson et al., 2006; Liu and Yin, 2016). This will balance the very different magnitudes of different time channels. Considering the relationship of  $\tilde{\mathbf{m}}$  and  $\mathbf{m}$  in equation 8, we can simplify the equations with all tildes omitted. By minimizing the penalty functional, we obtain the model updates using the Gauss-Newton method:

$$(\mathbf{J}^T \mathbf{J} + \gamma \mathbf{I}) \cdot \delta \mathbf{m} = \mathbf{J}^T \mathbf{r} - \gamma \mathbf{m}_l, \quad (9)$$

where  $\delta \mathbf{m}$  are the parameter updates,  $\mathbf{J}$  is the  $N_d \times M$  time-domain Jacobian matrix that is solved in a similar procedure in forward modelling using direct solver, the data residual is  $\mathbf{r} = \mathbf{d} - \mathbf{f}(\mathbf{m}_l)$  at  $l^{\text{th}}$  iteration. We use preconditioned conjugate gradient method to solve equation 9.

## NUMERICAL EXPERIMENTS

### Model data inversion

We first define conductors with different depths and geometries to test the accuracy and validity of our 3D inversion algorithm. The model is shown in Figure 2(a) where there are two conductive targets - a dipping plate and a rectangular conductor, with a resistivity of  $20 \Omega \cdot \text{m}$  and a strike length of 240m in  $y$  direction. The resistivity of the half-space is  $200 \Omega \cdot \text{m}$ . The survey system is a concentric loop system at 50 m height, with a half-sine transmitting wave and a base frequency of 30 Hz. We define 33 survey sites with 12 off-time channels and we have added 3% Gaussian noise to the data. We respectively conduct 3D and 1D inversions to the two conductors. The 3D inversion with field-separation method uses  $16 \times 16 \times 28$  grids in the VoI zone for each Tx-Rx pair, with a half-space as the starting model, while the 1D SVD inversion has a 8-layer starting model. The inversion results are shown in Figure 2(b) and 2(c).

From Figure 2, we can see that the results of 3D and 1D inversions have a good agreement with the reference model for the horizontal rectangular conductor, including the resistivity, shape and location. This is because the horizontal plate can be taken as a layered earth within a small area, considering the small footprint of the AEM system. The dipping plate has been recovered very well with 3D inversion, while 1D inversion appears unrelated to the dip, and performs as a deeper horizontal target instead. This shows that 3D inversion in this case is more accurate for 3D conductors, particularly for dipping targets for which 1D inversion cannot deliver good results. Figure 3 is a plot of the trade-off parameter, rms and penalty functional  $\varphi$  for 3D inversion. Quick convergence is obtained, with the final rms and  $\varphi$  are 1.06 and 1.09, respectively. The inversions for the present multi-conductor model

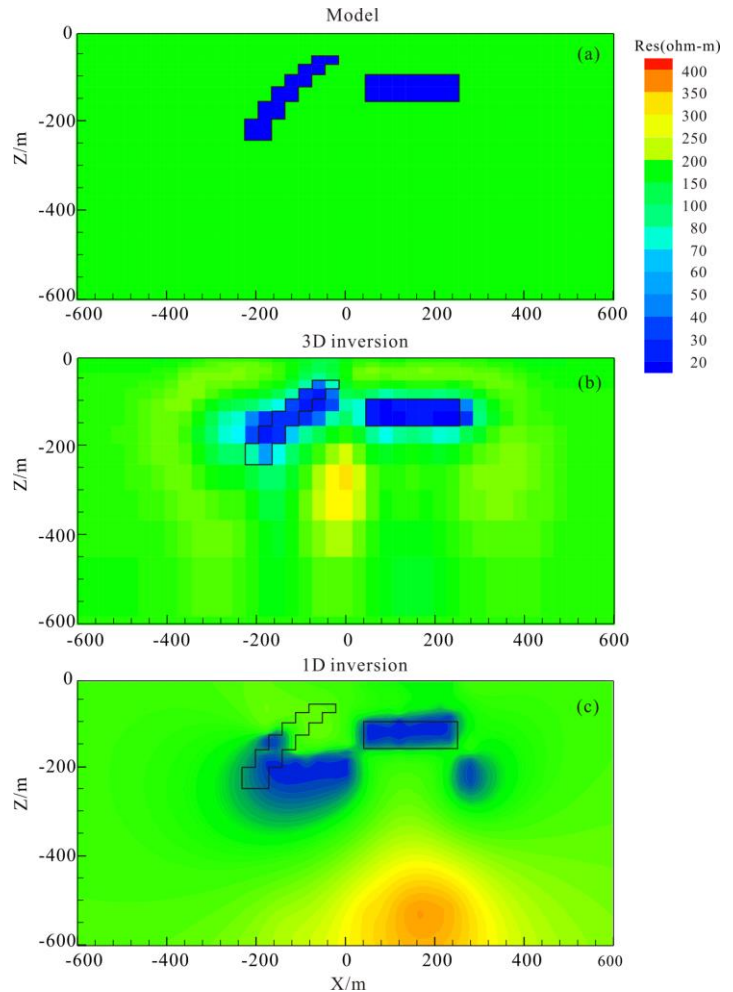


Figure 2: Theoretical model inversions.

demonstrate that our inversion algorithm has good sensitivity and resolution to the model, and 3D inversion has obvious advantages for non-layered conductors.

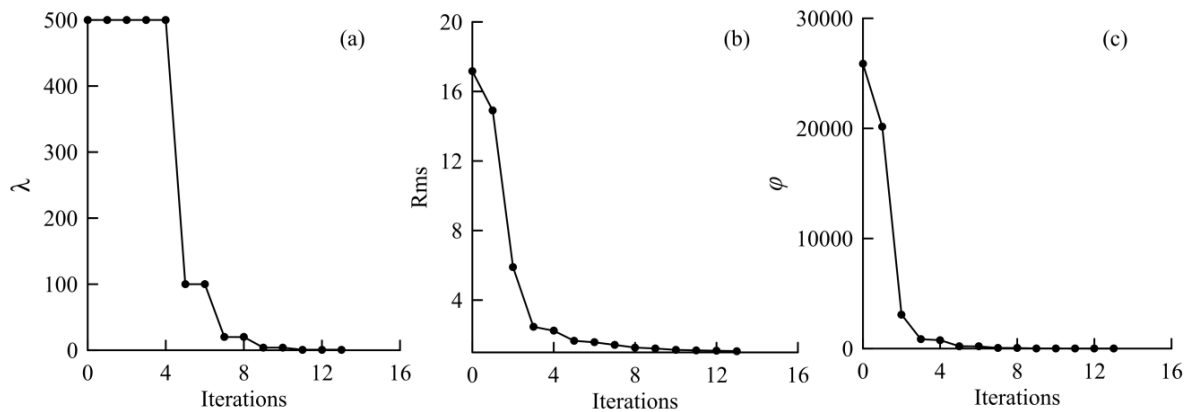


Figure 3: (a) Trade-off parameter; (b) normalized rms; (c) penalty functional  $\phi$ .

### Field data inversion

We have performed 1D and 3D inversions on the Lisheen deposit data acquired using a GEOTEM system in Ireland. The majority of the Lisheen deposit consists of Fe-Zn-Pb-Ag sulphides. Based on drilling results (Hitzman et al., 2002), the conductive minerals have a quasi-layer geometry. The system configuration for GEOTEM Tx-Rx offsets are respectively 131m, 0m, 50m in  $x, y, z$  directions. The base frequency is 75Hz, and the transmitting current is a half-sine with 2 ms on-time and 4.67 ms off-time. The flying height is around 100-150m and the survey zone is shown in Figure 4. The red areas in Figure 4 are the deposit. In this paper, we only show inversions of Line 5 data in our discussions.

For 3D inversion, we use  $16 \times 16 \times 20$  grids in each VoI zone and 100 time channels for theoretical calculation and interpolation for survey time channels. We adopt the SVD algorithm for 1D inversion. Figure 5(a) and 5(c) are the data fitting between the field data and predicted data respectively from 3D and 1D inversions, while Figure 5(b) and 5(d) are the corresponding recovered model for Line 5. In the airborne data, we can see that there is anomaly between 166250m and 167500m and the anomaly becomes larger from 166250m to 167500m, which is more obvious at early time channels than late ones. This corresponds in the recovered model to the conductive layer or conductors at a shallower depth around 167500m as shown in Figure 5(b) and 5(d). We can also see that the recovered results of 3D and 1D agree well, and both recover the conductors with similar depth (200-400m) and location, while the 3D inversion is consistent with the drilled sulphide locations and has associated a better fit to the data. The successful inversions of time-domain survey data further demonstrate the validity and effectiveness of our 3D inversion algorithm.

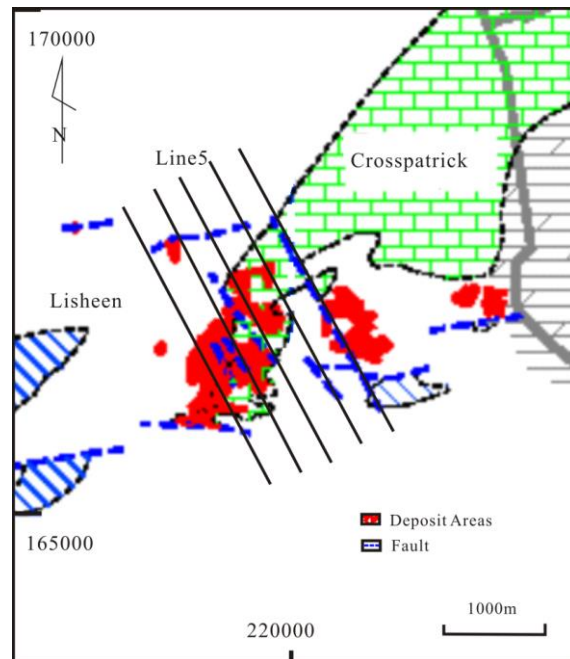
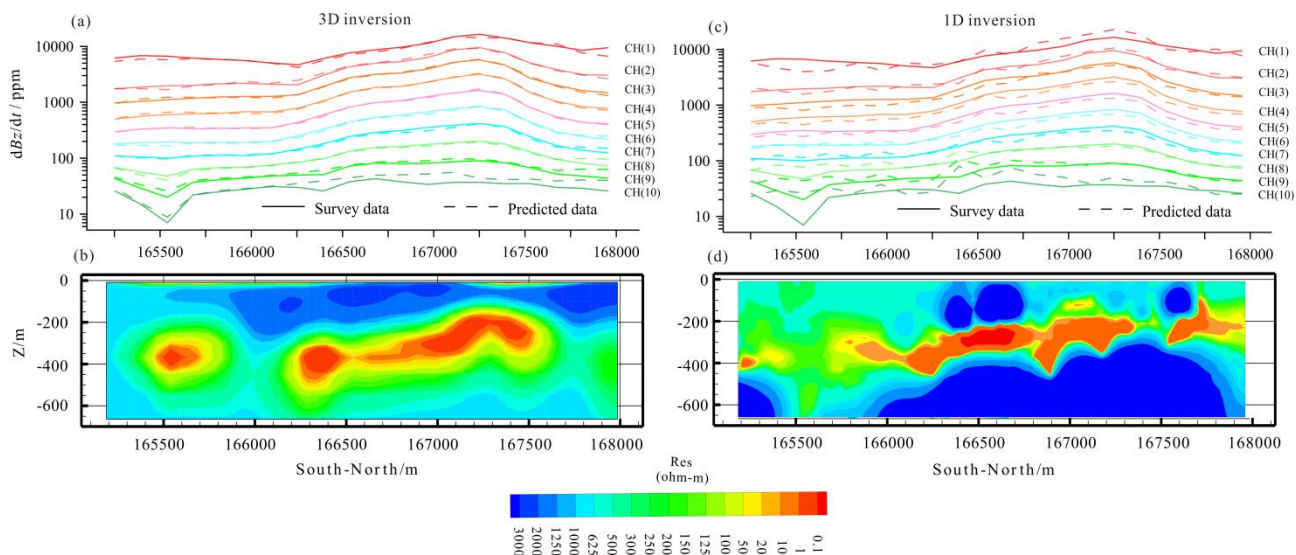


Figure 4: Location and lines of AEM survey (after Hitzman et al., 2002).



**Figure 5: Data fitting and recovered model for Line 5.**

(a) (c) are field data and final fitted response; (b) (d) are recovered models respectively from 3D inversion and 1D inversion.

## CONCLUSIONS

Combining the EM VoI of a secondary source with a local mesh and direct solver, we have conducted efficient forward modelling with the FV method. A direct Gauss-Newton optimization with pre-conditioned conjugate-gradient has also been successfully used in the 3D inversions. We tested 3D and 1D inversions on both synthetic model and field data. The model data inversions suggested that either 1D or 3D methods can recover a moderately extensive horizontal conductor, but only 3D inversion can recover a dipping plate-like conductor, which demonstrated the potential use of our 3D inversion, especially for irregular 3D conductors. Finally, the successful inversion of GEOTEM survey data from Lisheen deposit further conforms the effectiveness of our 3D inversion.

## ACKNOWLEDGMENTS

This paper has been financially supported by the Australian Society of Exploration Geophysicists Research Fund (RF16M06), the National Natural Science Foundation of China (41530320, 41774125), and the China Natural Science Foundation for Young Scientists (41404093), the Key National Research Project of China (2016YFC0303100, 2017YFC0601903). Project 2017033 was supported by Graduate Innovation Fund of Jilin University.

## REFERENCES

- Cai, J., Qi, Y. F., and Yin, C. C., 2014, Weighted laterally-constrained inversion of frequency-domain airborne EM data: Chinese Journal of Geophysics, 57, 953-960.
- Chen, J. P., and Raiche, A., 1998, Inverting AEM data using a damped eigenparameter method: Exploration Geophysics, 29, 128-132.
- Cox, L. H., and Zhdanov, M. S., 2007, Large scale 3D inversion of HEM data using a moving footprint: SEG Expanded Abstracts, San Antonio, 467-471.
- Cox, L. H., Wilson, G. A., and Zhdanov, M. S., 2010, 3D inversion of airborne electromagnetic data using a moving footprint: Exploration Geophysics, 41, 250-259. <http://www.Publish.Csiro.Au/nid/224/paper/EG10003.htm>
- Druyts, P., Craye, C., and Acheroy, M., 2010, Volume of Influence for Magnetic Soils and Electromagnetic Induction Sensors, IEEE transaction on Geoscience and Remote Sensing, 48, 3686-3697.
- Egbert, G. D., and Kelbert, A., 2012, Computational recipes for electromagnetic inverse problems: Geophysical Journal International, 189, 251-267.
- Hitzman, M. W., Redmond, P. B., and Beaty, D. W., 2002, The Carbonate-Hosted Lisheen Zn-Pb-Ag Deposit, County Tipperary, Ireland: Economic Geology, 97, 1627-1655.
- Jahandari, H., and Farquharson, C. G., 2014, A finite-volume solution to the geophysical electromagnetic forward problem using unstructured grids: Geophysics, 79, E287-E302.
- Ley-Cooper, A. Y., Macnae, J., and Viezzoli, A., 2010, Breaks in lithology: Interpretation problems when handling 2D structures with a 1D approximation: Geophysics, 75, WA179-WA188.
- Liu, G., and Becker, A., 1990, Two-dimensional mapping of sea-ice keels with airborne electromagnetics: Geophysics, 55, 239-248.
- Liu, Y., and Yin, C., 2016, 3D inversion for multipulse airborne transient electromagnetic data: Geophysics, 81, E401-E408.

- Macnae, J. C., Smith, R., Polzer, B. D., Lamontagne, Y., and Klinkert, P. S., 1991, Conductivity-depth imaging of airborne electromagnetic step-response data: *Geophysics*, 56, 102-114.
- Oldenburg, D. W., Haber, E., and Shekhtman, R., 2008, Forward Modelling and Inversion of Multi-Source TEM Data: SEG Expanded Abstracts, Las Vegas, 559-563.
- Oldenburg, D. W., Haber, E., and Shekhtman, R., 2013, Three dimensional inversion of multisource time domain electromagnetic data: *Geophysics*, 78, E47-E57.
- Reid, J. E., Pfaffling, A., and Vrbancich, J., 2006, Airborne electromagnetic footprints in 1D earths: *Geophysics*, 71, G63-G72.
- Ren, X., Yin, C., Liu, Y., Cai, J., Wang, C., and Ben, F., 2017, Efficient modeling of time-domain AEM using finite-volume method: *JEEG*, 22, 267-278.
- Vallée, M. A., and Smith, R. S., 2009, Application of Occam's inversion to airborne time-domain electromagnetics: *The Leading Edge*, 28, 284-287.
- Wilson, G. A., Raiche, A. P., and Sugeng, F., 2006, 2.5D inversion of airborne electromagnetic data: *Exploration Geophysics*, 37, 363-371.
- Yang, D., Oldenburg, D., and Haber, E., 2013, Massive parallelization of 3D electromagnetic inversion using local meshes: 5<sup>th</sup> International Symposium on Three-Dimensional Electromagnetics, Sapporo, Japan, 7-9.
- Yin, C., Huang, X., Liu, Y. H., and Cai, J., 2014, Footprint for frequency-domain airborne electromagnetic systems: *Geophysics*, 79, E243-E254.